UCRL-ID-133115

The Kinetic Tandem Concept: Theory and Computer Simulations of the Potential Barriers

R. F. Post

J. A. Byers

February 11, 1999

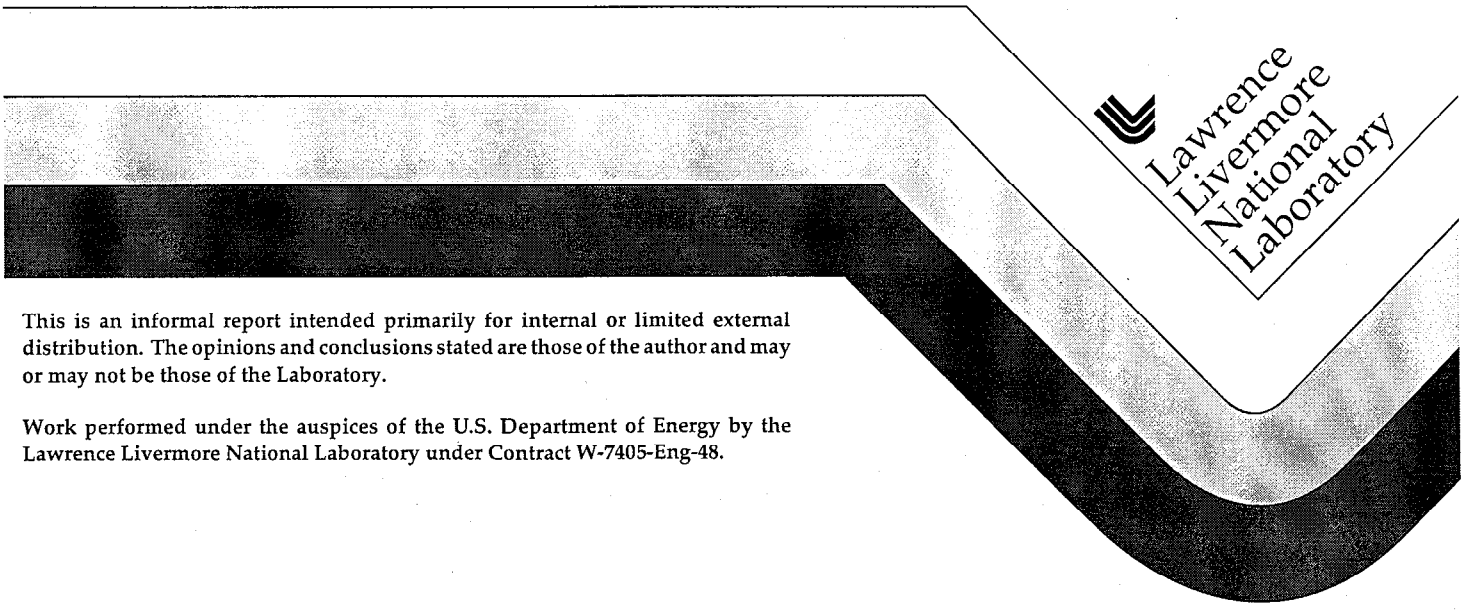

Work performed under the auspices of the U.S. Department of Energy by the Lawrence Livermore National Laboratory under Contract W-7405-Eng-48.

The Kinetic Tandem Concept: Theory and Computer Simulations of the Potential Barriers

Richard F. Post and Jack A. Byers
Lawrence Livermore National Laboratory

Abstract

The Kinetic Tandem fusion plasma confinement concept is a member of the class of "open" magnetic confinement systems whose magnetic topology is that of a tube of magnetic flux open at both ends. In open-ended systems the central problem is that of limiting the rate of plasma losses out the ends. In a conventional tandem mirror system end-plugging is accomplished by the generation of positive potential barriers within special short mirror cells located at each end of a long central confinement cell. The kinetic tandem concept accomplishes the same end result by employing dynamic effects, but without the necessity of special end cells. The field employed in the kinetic tandem is a simple axially symmetric solenoidal field whose intensity tapers to low values at the ends. Since the field line curvature is everywhere positive such a field is stabilizing for MHD interchange modes. Into each end are injected ion beams that are aimed nearly parallel to the field line direction. The ions from these beams then are radially compressed, stopped, and reflected back by magnetic mirror action in climbing up the magnetic gradient. In this way ion density peaks are formed between which the plasma is to be confined. As in the original tandem mirror concept, a localized ambipolar potential arises to maintain quasi-neutrality between the ions and the electrons. Provided the plasma density in the plugs is higher than that of the plasma contained between them the ions of the central plasma will be confined between the plugs by the positive potential barriers represented by the plugs. The plasma electrons will at the same time be confined by the overall positive potential of the plasma with respect to the ends. In this report some analytical calculations of the formation of the plugs will be given. These calculations were then confirmed and extended by computer simulations, using the LLNL code ICEPIC. Within the assumptions made in the theoretical calculations and in the code representation, fusion-relevant plug plasma parameters were achieved, and no evidence of unstable behavior was detected in the simulations.

I) Introduction

The kinetic tandem idea has been presented in previous papers [1,2]. It represents a method of creating a confinement system that mimics that of a conventional tandem mirror, but in a magnetic field of a "linear-collider" type, that is, an axially symmetric solenoidal field that is weakened at each end. In this section we will recapitulate the description of the kinetic tandem.

The tandem mirror concept involves "plugging" the end leakage of an open-ended field by creating localized regions of positive potential at each end of the system. In the original version of the tandem mirror [3,4] the plugging potentials were created by taking advantage of the ambipolar potential that arises spontaneously in open-ended systems in equalizing the rate of loss of ions and electrons. From the quasi-neutrality constraint in the plasma there arises the familiar Boltzmann-like expression for the potential difference, along the magnetic field lines, between two regions of the plasma at differing densities:

$$[e\phi(2) - e\phi(1)] = kT_e \ln\left[\frac{n_e(2)}{n_e(1)}\right] \qquad (1)$$

Thus in the original tandem-mirror concept small mirror cells, one at each end of the central mirror cell, were maintained at a higher plasma density than the plasma in the central cell, thereby creating a positive potential barrier inhibiting the escape of ions from the central cell. If the length of these cells was sufficiently short compared to that of the central cell the power required to maintain the plasmas in the plugs would be small compared to the fusion power generated in the central cell.

In the kinetic tandem concept there are no end mirror cells within which the higher-density plasma is maintained. Instead, a region of localized higher-density plasma near each end is to be created by the compression associated with the converging field lines of the solenoidal magnetic field. Ion beams are to be injected, near the ends of the long solenoid, nearly parallel to the direction of the field lines. Moving up the magnetic gradient these ions are compressed inward and eventually slowed to a stop and reflected by the field as it approaches its maximum value in the central, "confinement cell," region. Given a sufficiently high electron temperature of the lower-density plasma in the central region, a plugging potential adequate to contain the ions of that plasma will arise, inhibiting their escape. Again, if the plasma column between the plugging potentials is sufficiently long the fusion power released in the central region will be large enough compared to the power required to maintain the plugging potentials to yield a net useful power output.

The plugs of any tandem mirror system must perform two functions: The first is to provide a potential barrier that inhibits the escape of the ions of the central plasma. The second, and equally important, function is to balance the outward-directed parallel pressure of that plasma by an equal ingoing momentum flux. The mechanism for coupling this force is the positive gradient of the electric potential acting on the ions as they enter

the plugs. In the conventional tandem this momentum flux is taken up by the $\mu\nabla B$ (product of magnetic moment and gradient B) force on the plug ions as they are reflected by the end mirrors of the plug cells. In the kinetic tandem this pressure-balancing requirement must be satisfied by the inward momentum flux associated with the injected and reflected ions.

The two constraints just described - sufficiently high ion density to build the plug region, plus a sufficient inward momentum flux to balance the parallel pressure of the confined plasma - must be satisfied within the additional constraints of maintaining the stability of the plug ions against two MHD modes. The first of these is the firehose mode, previously discussed, where the limitation on ion density occurs near the point of injection. The second MHD mode that must be considered is the so-called "mirror" mode, where the region of concern is the density maximum of the mirror-reflected plug ions.

An approximate evaluation of the first two constraints - parallel pressure and plug ion density - may be obtained from simple mirror-physics relations. Ions of mass M_i(kg), injected at a current density j_0 (ions/m^2-sec.) at a velocity of v_0 (m/sec.) and at an angle to the direction of the magnetic field of θ_0(radians) produce an inwardly directed axial momentum flux that is, at first, increased by the convergence of the field lines, and then decreased as their perpendicular component of energy is increased through mirror action. As a result the parallel pressure reaches its maximum value at a field ratio that is 2/3 of that where reflection occurs, i.e. at a field ratio given by the relationship:

$$\frac{B(z)}{B(0)} = \frac{2}{3\sin^2(\theta_0)} \tag{2}$$

At this point the parallel pressure has the magnitude:

$$p_{par}\,(max) = \frac{2}{3\sqrt{3}} j_0\, M_i\, v_0 \left[\frac{1}{\sin^2(\theta_0)}\right] \tag{3}$$

At the maximum point the ion density from these ions has been compressed up to the value:

$$n_i = \frac{2j_0}{v_0}\left[\frac{1}{\sin^2(\theta_0)}\right] \quad \text{ions/m}^3 \tag{4}$$

For sufficiently small values of the injection angle and for ion source current densities of the order of those achieved experimentally [5], both the parallel pressure and the compressed ion density reach levels of practical interest. In what follows we will present more detailed evaluations of these quantities.

II) Analytic Calculation of Plug Parameters

Prior to the calculations made using a plasma simulation code, theory-based calculations were performed of the plasma properties and the parameters of the plugs of a tandem mirror. We will present the results of these calculations in the material in this and the next section.

To obtain a lowest-order answer to the density compression and the parallel pressure increase caused by the injection of a beam of ions into an increasing magnetic field the classical technique of employing a distribution function written in terms of the invariants of motion, namely, the specific energy, $\varepsilon = v^2/2$, and the specific magnetic moment, $\nu = v_\perp^2/2$ was employed. The angular dependence of the ion source function, $s(\theta)$ was chosen to be representative of realistic ion sources, while at the same time being integrable in terms of simple functions. The form chosen was:

$$s(\theta) = s_0[\sin^2(\theta) - \sin^2(\theta_1)]^2 [\sin^2(\theta_2) - \sin^2(\theta)]^2 \qquad (5)$$

Here θ_1 and θ_2 define the angular limits between which the ions are injected, with a gaussian-like current vs angle distribution as defined by the equation. A plot of this distribution function for typical values of the injection angle and angular width is shown in Figure 1.

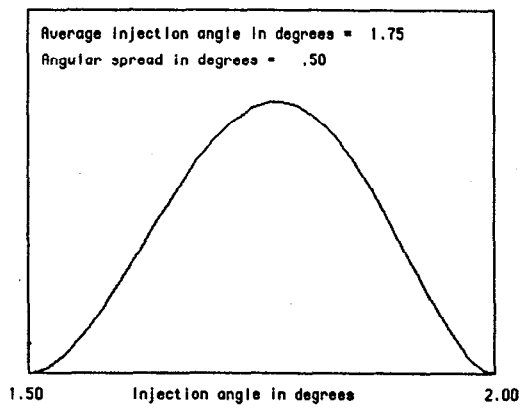

Figure 1: Source Angular Distribution

Inserting this distribution function into the expression for the density, integrating, and normalizing to the density at the position of the source results in plots of this density ratio as a function of the magnetic field intensity.

We first consider the case where the beams are monoenergetic. (This requirement is not a necessary one, and will be relaxed in later examples). For this first case the integrals to be performed to determine the density amplification caused by magnetic compression, and the parallel and perpendicular temperatures, are the following:

$$\text{Density:} \quad n(B) = \sqrt{2}\,\pi\, B \int_{\varepsilon} \int_{\nu} g(\nu,\varepsilon)(\varepsilon - \nu B)^{-1/2}\, d\nu d\varepsilon \qquad (6)$$

$$\text{Parallel pressure:} \quad P_{par} = 2\sqrt{2}\,\pi\, B \int_{\varepsilon} \int_{\nu} g(\nu,\varepsilon)(\varepsilon - \nu B)^{1/2}\, d\nu d\varepsilon \qquad (7)$$

$$\text{Perp. pressure:} \quad P_{perp} = \sqrt{2}\,\pi\, B^2 \int_{\varepsilon} \int_{\nu} g(\nu,\varepsilon)\nu(\varepsilon - \nu B)^{-1/2}\, d\nu d\varepsilon \qquad (8)$$

For this case the distribution function, $g(\nu,\varepsilon)$, is written as:

$$g(\nu,\varepsilon) = f(\varepsilon)s[\mu(\nu,\varepsilon)],$$

$$\text{with} \quad f(\varepsilon) = \delta(\varepsilon - \varepsilon_0),$$

$$\text{and} \quad \mu = \cos(\theta), \text{ so that } \mu^2 = 1 - \nu B/\varepsilon.$$

With the previously chosen functional form for $s(\mu)$ it can now be written as:

$$s(\mu) = s_0[\cos^2(\theta_1) - (1 - \nu B_0/\varepsilon)][(1 - \nu B_0/\varepsilon) - \cos^2(\theta_2)],$$

with the ν integration limits: $\nu_1 = \sin^2(\theta_1)(\varepsilon/B_0)$ and $\nu_2 = \sin^2(\theta_2)(\varepsilon/B_0)$.

Here B_0 is the value of B at the launching point of the injected ions.

Making the change of variables: $u = (\varepsilon - vB)$ the integrations may be performed in terms of simple quadratures, finding for the particle density as a function of magnetic field, n(B), the following lengthy expression:

$$n(B) = \sqrt{2}\,\pi\, s_0\, \varepsilon_0^{1/2} \left\{ \sqrt{A_1}\,[C_1+D_1+E_1+F_1+G_1] - \sqrt{A_2}\,[C_2+D_2+E_2+F_2+G_2] \right\} \quad (9)$$

$$A_{(1,2)} = [1 - \sin^2(\theta_{(1,2)})B/B_0]$$

$$C_{(1,2)} = \frac{2}{9}\left[\frac{B_0}{B}\right]^4 [A_{(1,2)}]^4$$

$$D_{(1,2)} = -\frac{4}{7}\left[\frac{B_0}{B}\right]^3 \left\{ \left[\frac{B_0}{B} - \sin^2(\theta_1) \right] + \left[\frac{B_0}{B} - \sin^2(\theta_2) \right] \right\} [A_{(1,2)}]^3$$

$$E_{(1,2)} = \frac{2}{5}\left[\frac{B_0}{B}\right]^2 \left\{ \left[\frac{B_0}{B} - \sin^2(\theta_1) \right]^2 + \left[\frac{B_0}{B} - \sin^2(\theta_2) \right]^2 + 4 \left[\frac{B_0}{B} - \sin^2(\theta_1) \right] \left[\frac{B_0}{B} - \sin^2(\theta_2) \right] \right\} \cdot$$

$$[A_{(1,2)}]^2$$

$$F_{(1,2)} = -\frac{4}{3}\left[\frac{B_0}{B}\right] \left\{ \left[\frac{B_0}{B} - \sin^2(\theta_1) \right]^2 \left[\frac{B_0}{B} - \sin^2(\theta_2) \right] + \left[\frac{B_0}{B} - \sin^2(\theta_1) \right] \left[\frac{B_0}{B} - \sin^2(\theta_2) \right]^2 \right\} \cdot$$

$$[A_{(1,2)}]$$

$$G_{(1,2)} = 2\left\{ \left[\frac{B_0}{B} - \sin^2(\theta_1) \right]^2 \left[\frac{B_0}{B} - \sin^2(\theta_2) \right]^2 \right\}$$

Our interest in the density variation with magnetic field is to determine the ratio of the peak particle density reached (following magnetic compression) to the input particle density at the mouth of the ion sources, i.e., we wish to determine $n(B)/n(B_0)$, the denominator being determined by setting $B = B_0$ in equation 9. The density ratio determined in this way must, however, be multiplied by a factor of two, to take into account that at every point beyond the ion source there exists a returning flux of particles, equal in magnitude and opposite in direction, as a result of the injected particles being reflected by mirror action.

For practically realizable source angular spreads the particle density compression ratios can be quite large, of order 10^4. Figure 2 is a plot of density compression ratio vs magnetic field ratio, for a case in which the angular spread, $(\theta_2 - \theta_1)$, is 0.5° and the mean injection angle, $(\theta_2 + \theta_1)/2$, is 1.75° . For this example case the peak density compression ratio is greater than 6000.

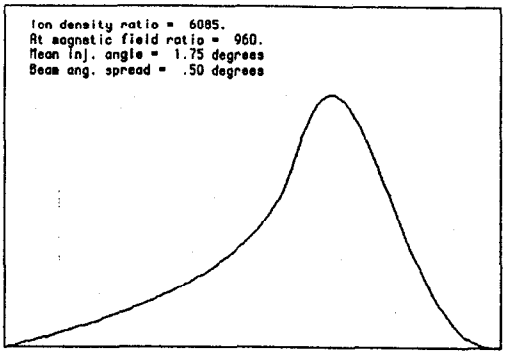

Figure 2: Density compression ratio vs magnetic field ratio

In a similar manner the parallel and perpendicular compression ratios can be determined, by evaluating the integrals in equations 7 and 8. For the parallel pressure we then have:

$$p_{par}(B) = 2\sqrt{2}\,\pi s_0 \varepsilon_0^{3/2} \{H_1 - H_2\} \tag{10}$$

$$H_{(1,2)} = \sqrt{A_{(1,2)}}\,\{J_{(1,2)} + K_{(1,2)} + L_{(1,2)} + M_{(1,2)} + N_{(1,2)}\}$$

$$J_{(1,2)} = \frac{9}{11}\,[A_{(1,2)}\,C_{(1,2)}]$$

$$K_{(1,2)} = \frac{7}{9}\,[A_{(1,2)}\,D_{(1,2)}]$$

$$L_{(1,2)} = \frac{5}{7}\,[A_{(1,2)}\,E_{(1,2)}]$$

$$M_{(1,2)} = \frac{3}{5}\,[A_{(1,2)}\,F_{(1,2)}]$$

$$N_{(1,2)} = \frac{1}{3}\,[A_{(1,2)}\,G_{(1,2)}]$$

In these equations the constants $A_{(1,2)}$ and $C_{(1,2)}$, etc. are defined as in equation 9.

A plot of $p_{par}(B)$ for the same source angular parameters as those in Figure 2 is shown in Figure 3. Note that p_{par} peaks at a lower magnetic field value than does n(B), as expected from the earlier discussion of equation 3.

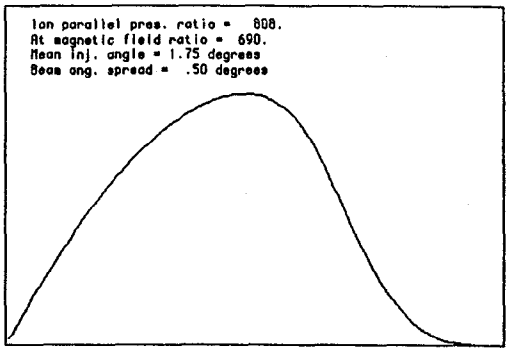

Figure 3: Parallel pressure ratio vs magnetic field ratio

The corresponding equations for the perpendicular pressure are as follows:

$$p_{perp}(B) = \sqrt{2}\,\pi s_0 \varepsilon_0^{3/2} \{I_1 - I_2\} \tag{11}$$

$$I_{(1,2)} = \sqrt{A_{(1,2)}}\,\{O_{(1,2)} + P_{(1,2)} + Q_{(1,2)} + R_{(1,2)} + S_{(1,2)}\}$$

$$O_{(1,2)} = \left\{1 - \frac{9}{11} A_{(1,2)}\right\} C_{(1,2)}$$

$$P_{(1,2)} = \left\{1 - \frac{7}{9} A_{(1,2)}\right\} D_{(1,2)}$$

$$Q_{(1,2)} = \left\{1 - \frac{5}{7} A_{(1,2)}\right\} E_{(1,2)}$$

$$R_{(1,2)} = \left\{1 - \frac{3}{5} A_{(1,2)}\right\} F_{(1,2)}$$

$$S_{(1,2)} = \left\{1 - \frac{1}{3} A_{(1,2)}\right\} G_{(1,2)}$$

A plot of $p_{perp}(B)$ is shown in Figure 4, for the same set of source angular parameters as those for the plots of Figures 2 and 3. Note that the pressure ratio reaches very high values, as a consequence of the combination of magnetic compression and the tipping of the velocity vectors of the ions from nearly parallel to the field lines to near-perpendicularity.

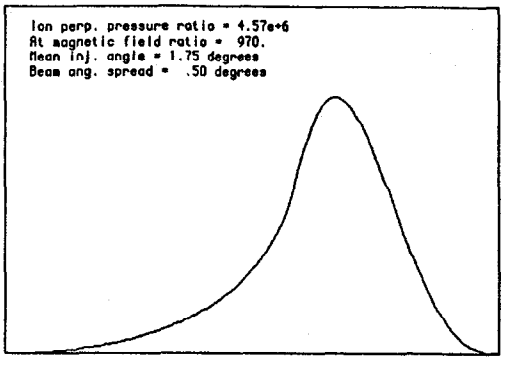

Figure 4: Perpendicular pressure ratio vs magnetic field ratio

The above analytical results for the density and pressure ratios can be used to determine a lowest-order calculation of the compressed values of these quantities, given the particle density at the sources. In a previous paper [2] these results were also incorporated into the stability criteria for the "firehose" and the "mirror" MHD modes to determine the limitations on the compressed densities and pressures that these modes imply, for given values of the source current density and intensity of the confining magnetic field. In this paper it was shown that fusion-relevant plasma parameters could be achieved at practically achievable levels of magnetic field and source current density.

In the application of these results to the generation of plugging potentials where the potential to be achieved is not negligible compared to the kinetic energy of the injected ions it is necessary to incorporate, self-consistently, the effect of that potential on the injected ions in modifying their orbits. In the next section we will describe a next-order calculation of this effect, using an iterative calculational method. However, the complexity of the problem is such that it requires the use of computer simulation methods to investigate the problem in greater depth. In a later section the results of such simulations will be presented and compared with those of the analytical approach.

III) Self-Consistent Calculation of Plug Densities by an Iterative Method

To calculate the compressed density of injected ions, including the effect on their orbits of an ambipolar potential, the integral expression for the density, equation 6, was first modified to include a potential, $\phi(B)$, i.e., varying spatially through its dependence on B. Through a coordinate transformation the integral was put in a form that was convenient for numerical integration. Then, setting the potential initially equal to zero,

the density ratio, $n(B)/n(B_0$, was calculated. First assuming a background electron temperature such that the ratio of the electron temperature to the injected ion energy is small, i.e., $(kT_e/W_i) << 1$, $\phi(B)$ was calculated, using the Boltzmann relationship, Equation 1. The density was then recalculated, forming the initial state for the next iteration. In the next iteration the electron temperature was increased incrementally, and a new density profile was calculated. This process was repeated until the desired ratio of electron temperature to ion energy was reached. As long as this ratio remained reasonably small it can be expected that the results would be an accurate representation of the self-consistent density and potential profiles. One clear limitation of the method is that it can only give predictions on the rising slope of n(B), since it requires that the potential be a single-valued function of B. This limitation is not present in the particle-in-cell computer simulations that are reported in a later section.

The modified form of Equation 6 is given by Equation 12 below:

$$n(B) = \sqrt{2}\,\pi\, B \int_{\varepsilon} \int_{\nu} g(\nu,\varepsilon)(\varepsilon - \phi(B) - \nu B)^{-1/2}\, d\nu d\varepsilon \qquad (12)$$

Making the transformations and change of variables: $\varepsilon = \varepsilon_0 = 1$ (normalized monoenergetic beams), normalizing the magnetic field by setting $B_0 = 1$, and defining the dimensionless variables, $x = B/B_0$, and $y(x) = \phi(B)/\varepsilon$, and making the substitution $u^2 = 1 - y(x) - \nu x$, Equation 12 then takes a singularity-free form suitable for numerical integration:

$$n(B) = 2\sqrt{2}\,\pi\, g_0 \int_a^b \left\{\cos^2(\theta_1) - \left[1 - \frac{1-u^2-y(x)}{x}\right]\right\}^2 \left\{\left[1 - \frac{1-u^2-y(x)}{x}\right] - \cos^2(\theta_2)\right\}^2 du \qquad (13)$$

Lower limit: $a = [1 - y(x) - \sin^2(\theta_2)]^{1/2}$; upper limit: $b = [1 - y(x) - \sin^2(\theta_1)]^{1/2}$.

The integral for $n(B_0)$ (where $\phi = 0$) then takes the much simpler form:

$$n(B_0) = 2\sqrt{2}\,\pi\, g_0 \int_{\cos(\theta_2)}^{\cos(\theta_1)} \left[\cos^2(\theta_1) - u^2\right]^2 \left[u^2 - \cos^2(\theta_2)\right]^2 du \qquad (18)$$

As a check on the results obtained with the analytic formulation, Equation 10, Equation 13 was numerically integrated with the electron temperature set equal to zero and with the same source angular parameters as those previously used. The two results were found to agree within the accuracy of the (trapezoidal rule) numerical integration algorithm that was employed. Following this the iterative method described above was used to determine the density distribution, as modified by the potentials associated with an electron temperature equal to 2.5 percent of the ion energy. For this case the peak potential was of order 2.5 log(6000) = 2.5 x 8.7 = 22 percent of the ion energy. The effect of this potential on the particle density was to form a "virtual anode" that, owing to the repulsion of the injected ions that it caused, moved the density peak back to somewhat lower magnetic field values. This effect is shown by the two curves plotted on Figure 5.

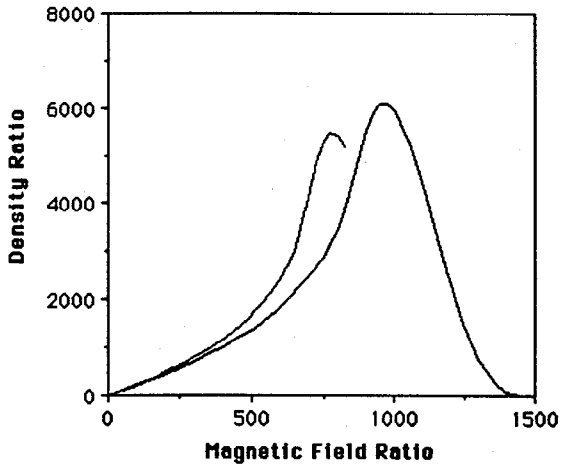

Figure 5: Effect of Self-Consistent Potential on Density Peak

In a practical application of the Kinetic Tandem advantage could be taken of the "virtual anode" effect to further enhance the density peak, and with it the plugging potential. For example, as the virtual anode built up in time the ion energies could be changed from a monoenergetic one to one chosen to maximize the number of ions turned around near the density peak, thus further amplifying the potential.

The effect of the virtual anode, including an effect of changing the ion energies, was also demonstrated in the computer simulations described in the next section.

IV) Computer Simulation Studies of the Plug Density

The computer simulations were performed using a modified version of an existing LLNL code. This code is an electrostatic 1-D particle-in-cell simulation code, ICEPIC (Inertial Confinement Electrostatic Particle In Cell), developed originally by Richard

Procassini. This code allows the input of several species of ions with differing charges and masses. Electrons can be treated either as particles or as a Boltzmann fluid. The axial motion of the particles is under the influence of $\mu\nabla B$ forces and forces from electrostatic fields of space-charge origin. An arbitrarily varying B(z) can be employed, read in from an input file. The code also has a particle-particle collision algorithm, a feature that was not required for the present problem because the single-bounce nature of the orbits of the ions rendered collisional effects unimportant. In the runs that were made the Boltzmann electron assumption was employed to determine potentials, as was the case with the iterative computational technique described in the previous section.

Summarizing the runs that were made using the simulation code, they were the following:

1. Proof-of-principle simulations: Injection of monoenergetic ions at small angles between 1.5 and 2.0 degrees into an axially increasing magnetic field, to compare the code results with those obtained by the analytic method.

   In the runs in which $kT_e = 0$, a steady-state was achieved in approximately one bounce time. The density ratio achieved, $n(B)/n(B_0) = 6000$ at $B/B_0 = 980$, agrees well with the analytical results for the same case.

   In subsequent runs, where kT_e was set equal to 6 percent of the energy of the injected ions, the location of the peak moved back down the magnetic gradient to $B/B_0 = 550$, behaving in the same manner as was observed in the iterative computations described in the previous section, but extending this regime to higher electron temperatures.

2. Time-dependent injection-velocity simulations: Starting with the same conditions as in the finite electron-temperature run in (1), the ion velocity was first increased by a factor 1.15. The ion velocity was then increased by another factor of 1.07, so that the kinetic energy of the ions was then about 1.5 times the original ion energy.

   Following the first increase in ion velocity (factor of 1.15) the peak density moved out from $B/B_0 = 550$ to $B/B_0 = 850$.

   With the second increase in velocity (factor of 1.07) the peak density moved out to $B/B_0 = 1050$.

   These runs confirmed and extended the "virtual anode" behavior seen in the iterative calculations of the previous section. As a result of this effect the maximum perpendicular velocity of the ions in the runs in (1) involving finite electron temperature was reduced to about 75 percent of that at injection. Following the second increase in ion velocity at injection the maximum

perpendicular velocity recovered to a value slightly larger than that seen in the first, zero electron temperature, runs.

3. Two-beam runs: In these runs two beams were used with different energies, but the same initial pitch-angle distribution.

In the first run, with $kT_e = 0$, the turning points of the two beams exactly overlapped, owing the fact that they had the same initial pitch-angle distribution.

In the next run a step-function increase in the electron temperature, to $kT_e = 6$ percent of the mean ion kinetic energy, was imposed. As a result the perfect overlapping of the turning points was perturbed, producing a wider density distribution and, as a consequence, a wider potential peak.

In all of the above runs there was no evidence of unstable behavior, suggesting that the plugs of the kinetic tandem should not be subject to instabilities of electrostatic origin. Another observation about the code and its behavior is that it behaved in a robust manner to step-function changes in the parameters. This result again suggests that the kinetic tandem plug formation process should be a stable one, even when the possibly destabilizing effects on the ion orbits of the ambipolar potential is present.

However, it should be said that to use plasma simulation methods to achieve a definitive proof of the stability of the plug formation process would likely require the use of a 3-D code that included magnetic and well as electrostatic effects of the kind that would be present in a real situation. Considering, however, that in the analytical computations the stability criteria for both the firehose and the mirror instabilities were shown to be satisfied for fusion-relevant plasma parameters, it is not unreasonable to assume that stable regimes would also be found in 3-D simulations.

V) Conclusion

Analytical formula for the calculation of the parameters of the plugs (ion-density peaks) in a kinetic tandem system have been presented and compared with computer simulations. Close agreement between the two approaches was found in the case where the ambipolar potential of the plug is small compared to the ion energy. Using the code, these results were extended to include the effects of a substantial "virtual anode" formed by the compressed and reflected ions and a population of electrons with kinetic energies several percent of the injected ion energies. In the computer simulations no evidence of unstable behavior of electrostatic origin was seen, and, provided criteria based on MHD theory are satisfied, the plugs should also be stable against both the firehose and mirror instabilities.

Acknowledgments

Valuable discussions with Dmitri Ryutov, Donald Pearlstein, and Tom Rognlien are gratefully acknowledged.

Work performed under the auspices of the U. S. Department of Energy by the Lawrence Livermore National Laboratory under contract no. W-7405-Eng-48

References

[1] R. F. Post, "Open Systems in the Quest for Fusion," *Plasma Physics Reports*, **23**, 816 (1997)

[2] R. F. Post, "Mirror-Based Fusion: Some Possible New Directions," *Transactions of Fusion Technology*, **35**, 40 (1999)

[3] G. I. Dimov, V. V. Zakaidov, M. E. Kishinevski, "Thermonuclear Confinement System with Twin Mirror Systems," *Sov. J. Plasma Phys.***2**, 326 (1976)

[4] T. K. Fowler, B. G. Logan, "The Tandem Mirror Reactor," *Comments Plasma Phys. Controlled Fusion*, **2**, 167 (1977)

[5] M. Dembinski, P. K. John, "Efficient Ion Extraction from a Flowing Plasma," *J. Appl. Phys*, **50**, 6113 (1979)